

ON THE CONTROL VOLUME FINITE ELEMENT METHODS AND THEIR APPLICATIONS TO MULTIPHASE FLOW

ZHANGXIN CHEN

Department of Mathematics, Box 750156
Southern Methodist University
Dallas, TX 75275-0156, USA

ABSTRACT. In this paper we systematically review the control volume finite element (CVFE) methods for numerical solutions of second-order partial differential equations. Their relationships to the finite difference and standard (Galerkin) finite element methods are considered. Through their relationship to the finite differences, upstream weighted CVFE methods and the conditions on positive transmissibilities (positive flux linkages) are studied. Through their relationship to the standard finite elements, error estimates for the CVFE are obtained. These estimates are comparable to those for the standard finite element methods using piecewise linear elements. Finally, an application to multiphase flows in porous media is presented.

1. Introduction. Finite difference, finite element, and finite volume methods are three numerical methods widely used in solving partial differential equations. Among them, the finite volume methods are the most intuitive because they are based on the local mass or energy conservation over volumes (control volumes or co-volumes). These methods lie somewhere between the finite element and finite difference methods. They possess grid flexibility analogous to that of the finite element methods, and they can be implemented in a way comparable to the finite difference methods.

The finite volume methods are also referred to as the control volume finite element methods [13, 25, 29], finite volume element methods [6, 35], and mixed covolume methods [16, 19]. They can be also seen as the finite element version of the cell-centered finite difference and box methods [5, 28, 39]. Regardless of their physical interpretations, the finite volume methods can be mathematically treated as Petrov-Galerkin methods with trial function spaces associated with certain finite element spaces and test spaces related to finite volumes.

Much research has been devoted to the error analysis of the finite volume methods for second-order elliptic and parabolic problems [6, 15, 18, 33]. Their error estimates of optimal order in the H^1 -norm are the same as those for the linear finite element method [23, 32, 34]. Their error estimates of optimal order in the L^2 -norm can be also derived [15, 23]. The finite volume methods for generalized Stokes problems were studied by many people [14, 16, 17, 19, 38, 41].

2000 *Mathematics Subject Classification.* Primary: 65N30, 65N10; Secondary: 76S05, 76T05.

Key words and phrases. Control volume finite element, Galerkin finite element, error analysis, upstream weighting, multiphase flow, numerical experiments.

In this paper we systematically review the finite volume methods, here termed the control volume finite element (CVFE) methods. For simplicity of the presentation, we focus on triangular elements. For rectangular elements, the reader may consult with [1]. We first write these methods in a finite difference formulation. It is known that transmissibility coefficients in this formulation must be positive. Positive transmissibilities or positive flux linkages always yield a direction of numerical fluxes in the physical direction. Negative transmissibilities are not physically meaningful, and generate unsatisfactory solutions. Here we discuss the condition on finite element grids that lead to positive transmissibilities.

We then consider upstream weighted CVFE methods. It is known that upstream weighting techniques are not easily incorporated into the standard finite element formulation. On the other hand, the CVFE formulation makes these techniques easy to incorporate. The CVFE methods without upstream weighting produce numerical fluxes continuous across the interfaces between control volumes. If upstream weighting is not properly introduced, the resulting CVFE methods may not preserve this physically important property. Here we discuss two types of upstream weighting strategies: potential- and flux-based, and we show that the former generates discontinuous fluxes across interfaces, while the latter produces continuous ones.

We next derive error estimates for the CVFE methods. To that end, we first establish their relationship to the standard finite element methods. Then, through this relationship error estimates for the CVFE are obtained. In particular, for piecewise linear elements, these two methods are of comparable accuracy.

Finally, we numerically test the CVFE methods. Numerical results support the theoretical analysis carried out in this paper. An application of the CVFE methods to multiphase flow in porous media is also presented.

The rest of the paper is organized as follows. In section 2, we state the partial differential problem and review the standard finite element methods. Then, in section 3 we define the basic CVFE methods. In section 4, we consider the condition required for positive transmissibilities. In section 5, upstream weighted CVFE methods are developed. An error analysis is given in section 6. In section 7, numerical experiments are performed. Finally, in section 8 concluding remarks are given.

2. Preliminaries. We consider the model problem

$$\begin{aligned} -\nabla \cdot (\mathbf{a}\nabla p) &= f && \text{in } \Omega, \\ p &= 0 && \text{on } \Gamma, \end{aligned} \quad (2.1)$$

where Ω is a bounded polygonal domain in the plane with boundary Γ . This equation can be thought of as a pressure equation in fluid flow in porous media [4, 22]. The coefficient tensor \mathbf{a} is assumed to be symmetric and positive definite:

$$0 < a_* \leq |\boldsymbol{\eta}|^2 \sum_{i,j=1}^2 a_{ij}(\mathbf{x})\eta_i\eta_j \leq a^* < \infty, \quad \mathbf{x} \in \Omega, \quad \boldsymbol{\eta} \neq \mathbf{0} \in \mathfrak{R}^2. \quad (2.2)$$

The right-hand side function f is in $L^2(\Omega)$. The usual Sobolev spaces $W^{l,q}(\Omega)$ with the norm $\|\cdot\|_{W^{l,q}(\Omega)}$ and the seminorm $|\cdot|_{W^{l,q}(\Omega)}$ [2] are used, where l is a nonnegative integer and $0 \leq q \leq \infty$. When $q = 2$, we simply write $H^l(\Omega) = W^{l,2}(\Omega)$. When $l = 0$, we have $L^2(\Omega) = H^0(\Omega)$. Below $(\cdot, \cdot)_Q$ denotes the $L^2(Q)$ inner product (Q is omitted if $Q = \Omega$).

Define

$$V = H_0^1(\Omega) = \{v \in H^1(\Omega) : v = 0 \text{ on } \Gamma\}.$$

A weak formulation of (2.1) is: Find $p \in V$ such that

$$a(p, v) = (f, v) \quad \forall v \in V, \tag{2.3}$$

where

$$a(p, v) = (\mathbf{a}\nabla p, \nabla v).$$

Because of assumption (2.2), problem (2.3) has a unique solution.

For $0 < h < 1$, let K_h be a shape-regular triangulation of Ω into triangles $\{K\}$ [20]. Associated with K_h , set

$$V_h = \{v \in H_0^1(\Omega) : v|_K \in P_1(K) \quad \forall K \in K_h\},$$

where $P_r(K)$ ($r \geq 0$) represents the space of polynomials of degree at most r on set K . The standard finite element method for (2.1) is: Find $p_h^s \in V_h$ such that

$$a(p_h^s, v) = (f, v) \quad \forall v \in V_h. \tag{2.4}$$

If the domain Ω is convex, it is known [20] that

$$\|p - p_h^s\|_{L^2(\Omega)} + h|p - p_h^s|_{H^1(\Omega)} \leq Ch^2|p|_{H^2(\Omega)}, \tag{2.5}$$

where C is a positive constant independent of h .

3. The Basic CVFE Methods. Control volumes can be constructed around grid nodes by joining the midpoints of the edges of a triangle with a point inside the triangle (cf. Fig. 1). Different locations of the point give rise to different forms of the flow term between grid nodes. When it is the barycenter of the triangle, the resulting grid is of CVFE type, and the resulting finite element methods are the CVFE methods. These methods were first introduced by Lemonnier (1979) for porous media flow simulation [29]. The CVFE grids are different from the PEBI (perpendicular bisection) grids (also called *Voronoi* grids [26]) in that the latter are locally orthogonal. The CVFE grids are more flexible. Hence, as an example, we study the CVFE methods.

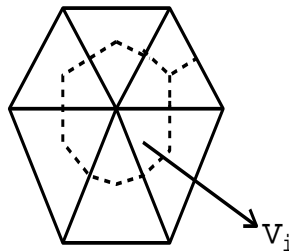


Fig. 1. A control volume.

Let V_i be a control volume. Replacing p by $p_h \in V_h$ in equation (2.1) and integrating over V_i , we see that

$$-\int_{V_i} \nabla \cdot (\mathbf{a}\nabla p_h) \, dx = \int_{V_i} f \, dx.$$

The divergence theorem implies

$$-\int_{\partial V_i} \mathbf{a}\nabla p_h \cdot \boldsymbol{\nu} \, d\ell = \int_{V_i} f \, dx, \tag{3.1}$$

where $\boldsymbol{\nu}$ is the outward unit normal to ∂V_i . Note that $\nabla p_h \cdot \boldsymbol{\nu}$ is continuous across each segment of ∂V_i (that lies inside a triangle). Thus, if \mathbf{a} is continuous across that segment, so is the flux $\mathbf{a} \nabla p_h \cdot \boldsymbol{\nu}$. Therefore, the flux is continuous across the edges of the control volume V_i . Furthermore, equation (3.1) indicates that the CVFE method is locally (i.e., on each control volume) conservative.

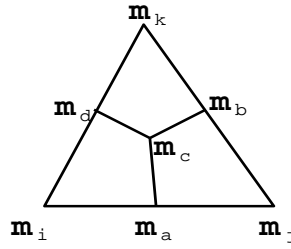


Fig. 2. A base triangle.

Given a triangle K with vertices \mathbf{m}_i , \mathbf{m}_j , and \mathbf{m}_k , edge midpoints \mathbf{m}_a , \mathbf{m}_b , and \mathbf{m}_d , and center \mathbf{m}_c (cf. Fig. 2), it follows that the approximation p_h to p on K is given by

$$p_h = p_i \lambda_i + p_j \lambda_j + p_k \lambda_k, \tag{3.2}$$

where the local basis functions λ_i are defined by

$$\lambda_i(\mathbf{m}_j) = \begin{cases} 1 & \text{if } i = j, \\ 0 & \text{if } i \neq j, \end{cases}$$

with

$$\lambda_i + \lambda_j + \lambda_k = 1. \tag{3.3}$$

They are the *barycentric coordinates* of the triangle K . Define

$$a_i = m_{j,2} - m_{k,2}, \quad b_i = -(m_{j,1} - m_{k,1}), \quad c_i = m_{j,1}m_{k,2} - m_{j,2}m_{k,1},$$

where $\mathbf{m}_i = (m_{i,1}, m_{i,2})$ and $\{i, j, k\}$ is cyclically permuted. Then the local basis functions λ_i , λ_j , and λ_k are given by

$$\begin{pmatrix} \lambda_i \\ \lambda_j \\ \lambda_k \end{pmatrix} = \frac{1}{2|K|} \begin{pmatrix} c_i & a_i & b_i \\ c_j & a_j & b_j \\ c_k & a_k & b_k \end{pmatrix} \begin{pmatrix} 1 \\ x_1 \\ x_2 \end{pmatrix},$$

where $|K|$ is the area of the triangle K . Consequently,

$$\frac{\partial \lambda_l}{\partial x_1} = \frac{a_l}{2|K|}, \quad \frac{\partial \lambda_l}{\partial x_2} = \frac{b_l}{2|K|}, \quad l = i, j, k. \tag{3.4}$$

We consider the computation of the left-hand side of equation (3.1) on $\mathbf{m}_a \mathbf{m}_c \mathbf{m}_d$ (cf. Fig. 2):

$$f_i \equiv - \int_{\mathbf{m}_a \mathbf{m}_c + \mathbf{m}_c \mathbf{m}_d} \mathbf{a} \nabla p_h \cdot \boldsymbol{\nu} \, dl. \tag{3.5}$$

On $\mathbf{m}_a \mathbf{m}_c$,

$$\boldsymbol{\nu} = \frac{(m_{c,2} - m_{a,2}, m_{a,1} - m_{c,1})}{|\mathbf{m}_a \mathbf{m}_c|},$$

and, on $\mathbf{m}_c \mathbf{m}_d$,

$$\boldsymbol{\nu} = \frac{(m_{d,2} - m_{c,2}, m_{c,1} - m_{d,1})}{|\mathbf{m}_c \mathbf{m}_d|},$$

where $|\mathbf{m}_a \mathbf{m}_c|$ denotes the length of edge $\mathbf{m}_a \mathbf{m}_c$. Consequently, if \mathbf{a} is a constant tensor on the triangle K , it follows from (3.2), (3.4), (3.5), the definition of a_i and b_i , and simple algebraic calculations that

$$f_i = |K| \sum_{l=i}^k \mathbf{a} \nabla \lambda_l \cdot \nabla \lambda_i p_l, \tag{3.6}$$

which shows that the CVFE and standard finite element methods using piecewise linear functions produce the same stiffness matrix (see section 6).

Using (3.3), equation (3.6) can be recast in the finite difference form

$$f_i = -T_{ij}(p_j - p_i) - T_{ik}(p_k - p_i), \tag{3.7}$$

where the *transmissibility coefficients* T_{ij} and T_{ik} are

$$T_{ij} = -|K| \mathbf{a} \nabla \lambda_j \cdot \nabla \lambda_i, \quad T_{ik} = -|K| \mathbf{a} \nabla \lambda_k \cdot \nabla \lambda_i.$$

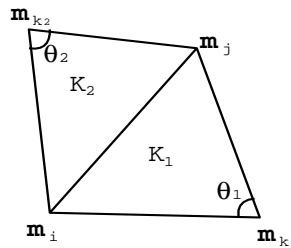


Fig. 3. Two adjacent triangles.

We now consider the assembly of the global transmissibility matrix. Each connection between any two adjacent nodes \mathbf{m}_i and \mathbf{m}_j includes the contributions from two triangles K_1 and K_2 that share the common edge with endpoints \mathbf{m}_i and \mathbf{m}_j (cf. Fig. 3). The transmissibility between \mathbf{m}_i and \mathbf{m}_j , where at least one of them is not on the external boundary, is

$$T_{ij} = - \sum_{l=1}^2 (|K_l| \mathbf{a} \nabla \lambda_j \cdot \nabla \lambda_i) \Big|_{K_l}. \tag{3.8}$$

Applying equations (3.1) and (3.7), we obtain the linear system on the control volume V_i in terms of pressure values at the vertices of triangles

$$- \sum_{j \in \Omega_i} T_{ij} (p_j - p_i) = F_i, \tag{3.9}$$

where Ω_i is the set of all neighboring nodes of \mathbf{m}_i and $F_i = \int_{V_i} f \, dx$.

The above result is summarized in the next theorem.

Theorem 3.1. *With \mathbf{a} being piecewise constant on K_h and the transmissibility coefficient T_{ij} between nodes \mathbf{m}_i and \mathbf{m}_j being defined in (3.8), system (3.1) can be written in terms of the finite difference formulation (3.9).*

If ∂V_i contains a part of the Dirichlet boundary in (2.1), then the pressure on the corresponding part is given. If a Neumann boundary condition is imposed in (2.1), then the flux on the part of the Neumann boundary ∂V_i is known. The third (mixed type) boundary condition can be also easily incorporated.

4. Positive Transmissibilities. The transmissibility coefficient T_{ij} defined in (3.8) must be positive. Positive transmissibilities or positive flux linkages always yield a direction of numerical fluxes in the physical direction. Negative transmissibilities are not physically meaningful, and generate unsatisfactory solutions.

For simplicity, we consider a *homogeneous anisotropic* medium: $\mathbf{a} = \text{diag}(a_{11}, a_{22})$ (i.e., a_{11} and a_{22} are positive constants). In this case, using (3.4) and (3.6), T_{ij} restricted to each triangle K (cf. Fig. 3) is

$$T_{ij} = -\frac{a_{11}a_j a_i + a_{22}b_j b_i}{4|K|}.$$

Introduce a coordinate transform:

$$x'_1 = \frac{x_1}{\sqrt{a_{11}}}, \quad x'_2 = \frac{x_2}{\sqrt{a_{22}}}. \tag{4.1}$$

Under this transform, the area of the transformed triangle K' is

$$|K'| = \frac{|K|}{\sqrt{a_{11}a_{22}}}.$$

Consequently, T_{ij} becomes

$$T_{ij} = \sqrt{a_{11}a_{22}} \frac{|\mathbf{m}_{k'} \mathbf{m}_{j'}| |\mathbf{m}_{k'} \mathbf{m}_{i'}| \cos \theta_{k'}}{4|K'|} = \sqrt{a_{11}a_{22}} \frac{\cot \theta_{k'}}{2},$$

where $\theta_{k'}$ is the angle of the triangle at node $\mathbf{m}_{k'}$ in the transformed plane. Because each global transmissibility consists of the contributions from two adjacent triangles, the global T_{ij} between nodes \mathbf{m}_i and \mathbf{m}_j (cf. Fig. 3) is

$$T_{ij} = \sqrt{a_{11}a_{22}} \left(\frac{\cot \theta_{k'_1} + \cot \theta_{k'_2}}{2} \right), \tag{4.2}$$

where $\theta_{k'_1}$ and $\theta_{k'_2}$ are the opposite angles of the two triangles. Thus the requirement $T_{ij} > 0$ is equivalent to

$$\theta_{k'_1} + \theta_{k'_2} < \pi. \tag{4.3}$$

For an edge on the external boundary, the requirement is

$$\theta_{k'} < \pi/2. \tag{4.4}$$

Note that all these angles are measured in the (x'_1, x'_2) -coordinate plane.

Theorem 4.1. *Assume that $\mathbf{a} = \text{diag}(a_{11}, a_{22})$ with positive constants a_{11} and a_{22} . Then the requirement $T_{ij} > 0$ is equivalent to condition (4.3). For an edge on the external boundary, condition (4.4) is required.*

It is interesting to note that condition (4.3) is related to a Delaunay triangulation. A Delaunay triangulation satisfies the empty circle criterion: The circumcircle of each triangle must not contain any other nodes in its interior. Given a shape-regular triangulation K_h of a convex domain, K_h can be converted to a Delaunay triangulation in a sequence of local edge swaps as follows [21, 27]: Each internal edge in K_h is examined. If it is a part of a convex quadrilateral (cf. Fig. 3), then the circumcircles of the two triangles are checked. If one of the circumcircles contains the fourth vertex of the quadrilateral, then the diagonal of this quadrilateral is swapped (cf. Fig. 4). The resulting local triangulation then satisfies the empty circle criterion, i.e., the *local optimality condition* [21, 27]. A sequence of local edge swaps eventually converges, so that every internal edge is locally optimal. All internal edges of a triangulation are locally optimal if and only if it is a Delaunay triangulation [27].

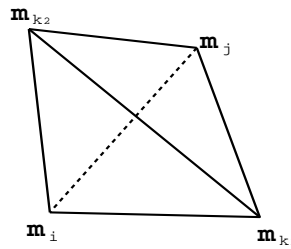


Fig. 4. An edge swap.

On the other hand, the local optimal condition is equivalent to condition (4.3) [21]. Hence the edge swapping procedure can be given geometrically: Given a shape-regular triangulation K_h , if the sum of the two angles opposite edge $\mathbf{m}_i \mathbf{m}_j$ (cf. Fig. 3) is larger than π , then this edge is replaced by edge $\mathbf{m}_{k_1} \mathbf{m}_{k_2}$. This edge swap can be only carried out if the quadrilateral is convex. If it is not, then condition (4.3) must necessarily be true. For a convex domain, no addition or movement of nodes is required to convert K_h to a Delaunay triangulation.

For problem (2.1), the edge swapping procedure can be generalized [24]: Each edge $\mathbf{m}_i \mathbf{m}_j$ is examined, and the transmissibility T_{ij} is computed using equation (3.8). If T_{ij} is negative, then this edge is replaced by $\mathbf{m}_{k_1} \mathbf{m}_{k_2}$. If the solution domain is convex and \mathbf{a} is constant, this procedure is equivalent to establishing a Delaunay triangulation in the (x'_1, x'_2) plane where \mathbf{a}' is the identity tensor. The equivalence of positive transmissibilities with a Delaunay triangulation is true only for internal edges in the transformed plane when \mathbf{a} is constant. In general, a Delaunay triangulation of the physical plane cannot ensure positive transmissibilities, even for internal edges. However, because most domains that arise in practical applications can be treated as a union of convex regions with a constant permeability tensor \mathbf{a} , the local edge swap procedure should tend to minimize the number of internal edges having negative transmissibilities.

In general, edges on the external boundary of a domain can have negative transmissibilities. This problem can be overcome by adding a boundary node as in Fig. 5. Suppose that $T_{ij} < 0$ on edge $\mathbf{m}_i \mathbf{m}_j$; i.e., in the (x'_1, x'_2) plane, the angle opposite this edge is larger than $\pi/2$. A new node is added at the intersection of $\mathbf{m}_i \mathbf{m}_j$ with the orthogonal line segment to $\mathbf{m}_i \mathbf{m}_j$ drawn from \mathbf{m}_k . Note that there is no edge swap for a boundary edge.

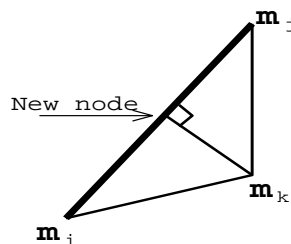


Fig. 5. An addition of a new boundary node.

5. Upstream Weighted CVFE Methods. The basic idea of upstream weighting is to choose the value of a property coefficient according to the upstream direction

of a flux. This idea has been used in upwind finite difference methods [4]. In this section, we consider two upstream weighting strategies for equation (3.9): potential- and flux-based.

5.1. The potential-based upstream weighting scheme. Suppose that equation (2.1) is of the form

$$-\nabla \cdot (\lambda \mathbf{a} \nabla p) = f(x_1, x_2) \quad \text{in } \Omega, \quad (5.1)$$

where \mathbf{a} and λ are a permeability tensor and a mobility coefficient, respectively, in porous media flow, for example. For this problem, a CVFE analogue to (3.9) can be derived. If \mathbf{a} is a scalar a and is different on the two sides of an edge of V_i , across that edge it should be approximated by the harmonic average

$$a(\mathbf{x}) = \frac{2a^+(\mathbf{x})a^-(\mathbf{x})}{a^+(\mathbf{x}) + a^-(\mathbf{x})},$$

where a^+ and a^- indicate the respective values from the two sides. The reason for using a harmonic average is that for an inactive node (i.e., the node where $a = 0$), this average gives the correct value (i.e., $a = 0$), in contrast with the arithmetic average. If \mathbf{a} is a tensor, this harmonic average is used for each component of \mathbf{a} and the result is denoted by \mathbf{a}_{har} . For the mobility coefficient λ , in practice, upstream weighting must be used to maintain stability for the CVFE methods. As a result of these two observations, the transmissibility between nodes \mathbf{m}_i and \mathbf{m}_j restricted to each triangle K becomes

$$T_{ij} = -|K| \lambda_{ij}^{up} \mathbf{a}_{har} \nabla \lambda_j \cdot \nabla \lambda_i, \quad (5.2)$$

where the potential-based upstream weighting scheme is defined by

$$\lambda_{ij}^{up} = \begin{cases} \lambda(\mathbf{m}_i) & \text{if } p_i > p_j, \\ \lambda(\mathbf{m}_j) & \text{if } p_i < p_j. \end{cases} \quad (5.3)$$

In fact, it is a pressure-based approach in the current context. The name ‘‘potential-based’’ is due to the fact that potentials are usually used in place of p in porous media flow simulation.

This potential-based upstream weighting scheme is easy to implement. However, it violates the important flux continuity property across the interfaces between control volumes. To see this, consider the case $\mathbf{a} = \text{diag}(a_{11}, a_{22})$, where \mathbf{a} is a constant diagonal tensor on the triangle K (cf. Fig. 2). Applying (3.4) and (5.2), the flux on edge $\mathbf{m}_a \mathbf{m}_c$ is

$$\begin{aligned} f_{i, \mathbf{m}_a \mathbf{m}_c} &= -\lambda_{ij}^{up} \left(a_{11}(m_{c,2} - m_{a,2}) \frac{\partial \lambda_j}{\partial x_1} + a_{22}(m_{a,1} - m_{c,1}) \frac{\partial \lambda_j}{\partial x_2} \right) (p_j - p_i) \\ &\quad - \lambda_{ik}^{up} \left(a_{11}(m_{c,2} - m_{a,2}) \frac{\partial \lambda_k}{\partial x_1} + a_{22}(m_{a,1} - m_{c,1}) \frac{\partial \lambda_k}{\partial x_2} \right) (p_k - p_i), \end{aligned}$$

and on edge $\mathbf{m}_c \mathbf{m}_d$,

$$\begin{aligned} f_{i, \mathbf{m}_c \mathbf{m}_d} &= -\lambda_{ij}^{up} \left(a_{11}(m_{d,2} - m_{c,2}) \frac{\partial \lambda_j}{\partial x_1} + a_{22}(m_{c,1} - m_{d,1}) \frac{\partial \lambda_j}{\partial x_2} \right) (p_j - p_i) \\ &\quad - \lambda_{ik}^{up} \left(a_{11}(m_{d,2} - m_{c,2}) \frac{\partial \lambda_k}{\partial x_1} + a_{22}(m_{c,1} - m_{d,1}) \frac{\partial \lambda_k}{\partial x_2} \right) (p_k - p_i). \end{aligned}$$

Similarly, the fluxes on edges $\mathbf{m}_b\mathbf{m}_c$ and $\mathbf{m}_c\mathbf{m}_a$ at node \mathbf{m}_j are, respectively,

$$f_{j,\mathbf{m}_b\mathbf{m}_c} = -\lambda_{jk}^{up} \left(a_{11}(m_{c,2} - m_{b,2}) \frac{\partial \lambda_k}{\partial x_1} + a_{22}(m_{b,1} - m_{c,1}) \frac{\partial \lambda_k}{\partial x_2} \right) (p_k - p_j) \\ - \lambda_{ji}^{up} \left(a_{11}(m_{c,2} - m_{b,2}) \frac{\partial \lambda_i}{\partial x_1} + a_{22}(m_{b,1} - m_{c,1}) \frac{\partial \lambda_i}{\partial x_2} \right) (p_i - p_j),$$

and

$$f_{j,\mathbf{m}_c\mathbf{m}_a} = -\lambda_{jk}^{up} \left(a_{11}(m_{a,2} - m_{c,2}) \frac{\partial \lambda_k}{\partial x_1} + a_{22}(m_{c,1} - m_{a,1}) \frac{\partial \lambda_k}{\partial x_2} \right) (p_k - p_j) \\ - \lambda_{ji}^{up} \left(a_{11}(m_{a,2} - m_{c,2}) \frac{\partial \lambda_i}{\partial x_1} + a_{22}(m_{c,1} - m_{a,1}) \frac{\partial \lambda_i}{\partial x_2} \right) (p_i - p_j),$$

and the fluxes on edges $\mathbf{m}_d\mathbf{m}_c$ and $\mathbf{m}_c\mathbf{m}_b$ at node \mathbf{m}_k are, respectively,

$$f_{k,\mathbf{m}_d\mathbf{m}_c} = -\lambda_{ki}^{up} \left(a_{11}(m_{c,2} - m_{d,2}) \frac{\partial \lambda_i}{\partial x_1} + a_{22}(m_{d,1} - m_{c,1}) \frac{\partial \lambda_i}{\partial x_2} \right) (p_i - p_k) \\ - \lambda_{kj}^{up} \left(a_{11}(m_{c,2} - m_{d,2}) \frac{\partial \lambda_j}{\partial x_1} + a_{22}(m_{d,1} - m_{c,1}) \frac{\partial \lambda_j}{\partial x_2} \right) (p_j - p_k),$$

and

$$f_{k,\mathbf{m}_c\mathbf{m}_b} = -\lambda_{ki}^{up} \left(a_{11}(m_{b,2} - m_{c,2}) \frac{\partial \lambda_i}{\partial x_1} + a_{22}(m_{c,1} - m_{b,1}) \frac{\partial \lambda_i}{\partial x_2} \right) (p_i - p_k) \\ - \lambda_{kj}^{up} \left(a_{11}(m_{b,2} - m_{c,2}) \frac{\partial \lambda_j}{\partial x_1} + a_{22}(m_{c,1} - m_{b,1}) \frac{\partial \lambda_j}{\partial x_2} \right) (p_j - p_k).$$

For the flux to be continuous across edge $\mathbf{m}_a\mathbf{m}_c$, it is required that $f_{i,\mathbf{m}_a\mathbf{m}_c} + f_{j,\mathbf{m}_c\mathbf{m}_a} = 0$; i.e.,

$$-\lambda_{ij}^{up} \left(a_{11}(m_{c,2} - m_{a,2}) \frac{\partial \lambda_j}{\partial x_1} + a_{22}(m_{a,1} - m_{c,1}) \frac{\partial \lambda_j}{\partial x_2} \right) (p_j - p_i) \\ - \lambda_{ik}^{up} \left(a_{11}(m_{c,2} - m_{a,2}) \frac{\partial \lambda_k}{\partial x_1} + a_{22}(m_{a,1} - m_{c,1}) \frac{\partial \lambda_k}{\partial x_2} \right) (p_k - p_i) \\ - \lambda_{jk}^{up} \left(a_{11}(m_{a,2} - m_{c,2}) \frac{\partial \lambda_k}{\partial x_1} + a_{22}(m_{c,1} - m_{a,1}) \frac{\partial \lambda_k}{\partial x_2} \right) (p_k - p_j) \\ - \lambda_{ji}^{up} \left(a_{11}(m_{a,2} - m_{c,2}) \frac{\partial \lambda_i}{\partial x_1} + a_{22}(m_{c,1} - m_{a,1}) \frac{\partial \lambda_i}{\partial x_2} \right) (p_i - p_j) = 0.$$

Because it must be satisfied for all choices of \mathbf{a} , this equation reduces to

$$a_{11}(m_{a,2} - m_{c,2}) \left[\lambda_{ij}^{up} \frac{\partial \lambda_j}{\partial x_1} (p_j - p_i) + \lambda_{ji}^{up} \frac{\partial \lambda_i}{\partial x_1} (p_j - p_i) \right. \\ \left. + \lambda_{ik}^{up} \frac{\partial \lambda_k}{\partial x_1} (p_k - p_i) + \lambda_{jk}^{up} \frac{\partial \lambda_k}{\partial x_1} (p_j - p_k) \right] = 0,$$

and

$$a_{22}(m_{c,1} - m_{a,1}) \left[\lambda_{ij}^{up} \frac{\partial \lambda_j}{\partial x_2} (p_j - p_i) + \lambda_{ji}^{up} \frac{\partial \lambda_i}{\partial x_2} (p_j - p_i) \right. \\ \left. + \lambda_{ik}^{up} \frac{\partial \lambda_k}{\partial x_2} (p_k - p_i) + \lambda_{jk}^{up} \frac{\partial \lambda_k}{\partial x_2} (p_j - p_k) \right] = 0.$$

For these two equations to hold simultaneously for any type of triangle, the only possibility is

$$p_k \geq p_i = p_j.$$

In the same manner, we can prove

$$p_i \geq p_j = p_k \quad \text{and} \quad p_j \geq p_i = p_k.$$

Hence, for the flux to be continuous across the edges of control volumes, $p_i = p_j = p_k$. That is, the flux is continuous across the edges of all control volumes if and only if the approximate solution p_h has the same value at all vertices, which is generally not true. Therefore, in general, the potential-based upstream weighted CVFE methods generate a discontinuous flux across the edges of control volumes.

Theorem 5.1. *The potential-based upstream weighting scheme (5.3) generates a discontinuous flux across the edges of control volumes unless the approximate solution p_h has the same value at all vertices.*

On the other hand, the above argument leads to another upstream weighting strategy: flux-based.

5.2. The flux-based upstream weighting scheme. For the flux-based approach, the upstream direction is determined by the sign of a flux. It follows from (3.5) and (5.2) that the flux on edge $\mathbf{m}_a\mathbf{m}_c$ at node \mathbf{m}_i (cf. Fig. 2) is

$$f_{i,\mathbf{m}_a\mathbf{m}_c} = - \sum_{l=i}^k \lambda^{up} \mathbf{a}_{har} \nabla \lambda_l \cdot (m_{c,2} - m_{a,2}, m_{a,1} - m_{c,1}) p_l,$$

and, at node \mathbf{m}_j ,

$$f_{j,\mathbf{m}_c\mathbf{m}_a} = - \sum_{l=i}^k \lambda^{up} \mathbf{a}_{har} \nabla \lambda_l \cdot (m_{a,2} - m_{c,2}, m_{c,1} - m_{a,1}) p_l,$$

where the upstream weighting is now defined by

$$\lambda^{up} = \begin{cases} \lambda(\mathbf{m}_i) & \text{if } f_{i,\mathbf{m}_a\mathbf{m}_c} > 0, \\ \lambda(\mathbf{m}_j) & \text{if } f_{i,\mathbf{m}_a\mathbf{m}_c} < 0. \end{cases} \tag{5.4}$$

From this definition it follows that

$$f_{i,\mathbf{m}_a\mathbf{m}_c} + f_{j,\mathbf{m}_c\mathbf{m}_a} = 0. \tag{5.5}$$

The fluxes on other edges can be defined in the same fashion. It is evident from (5.5) that the flux-based upstream weighted CVFE methods have a continuous flux across the edges of control volumes.

Theorem 5.2. *The flux-based upstream weighting scheme (5.4) generates a continuous flux across the edges of control volumes.*

6. Error Analysis for the CVFE Methods. To derive an error estimate for the CVFE methods, we write equation (3.1) in a more slightly general form. For simplicity, let \mathbf{a} be the identity tensor. For a variable coefficient \mathbf{a} , the result in this section remains valid if \mathbf{a} is projected into the space of piecewise constants associated with K_h as in the treatment of the standard finite element methods [8] (also refer to equation (3.6)).

Let \mathcal{K}_h be the set of all control volumes $\{V_i\}$, and W_h be the space of piecewise constants with respect to \mathcal{K}_h whose elements vanish on Γ . Let $\{\varphi_i\}$ denote the usual nodal basis for V_h that satisfies

$$\varphi_i(\mathbf{x}_j) = \delta_{ij},$$

where \mathbf{x}_j is a vertex in the triangulation K_h . Also, let $\{\psi_i\}$ indicate the basis for W_h that consists of the characteristic functions:

$$\psi_i(\mathbf{x}) = \begin{cases} 1 & \text{if } \mathbf{x} \in V_i, \\ 0 & \text{otherwise.} \end{cases}$$

Note that the dimensions of V_h and W_h are the same. Furthermore, there exists an invertible mapping G from V_h onto W_h : For

$$v(\mathbf{x}) = \sum_i v_i \varphi_i(\mathbf{x}), \quad \mathbf{x} \in \Omega,$$

we define $G(v) = \hat{v} \in W_h$ by

$$G(v) = \hat{v} = \sum_i v_i \psi_i(\mathbf{x}), \quad \mathbf{x} \in \Omega.$$

Note that v and \hat{v} have the same values at the vertices in K_h . With this mapping, we see that $\psi_i = \hat{\varphi}_i = G(\varphi_i)$.

Introduce the bilinear form

$$\hat{a}(p_h, w) = - \sum_{V_i \in \mathcal{K}_h} \int_{\partial V_i} \nabla p_h \cdot \boldsymbol{\nu} w \, dl, \quad w \in W_h.$$

Now, method (3.1) is equivalently defined: Find $p_h \in V_h$ such that

$$\hat{a}(p_h, w) = (f, w) \quad \forall w \in W_h. \tag{6.1}$$

To see a relationship between method (2.4) and method (6.1), we prove the next lemma.

Lemma 6.1. *With $\mathbf{a} = \mathbf{I}$ (the identity tensor),*

$$\hat{a}(p_h, \hat{v}) = a(p_h, v) \quad \forall v \in V_h. \tag{6.2}$$

Proof. It suffices to show (6.2) with $v = \varphi_i$ (thus $\hat{v} = \hat{\varphi}_i = \psi_i$). Set

$$p_h = \sum_l p_l \varphi_l.$$

Then we see that

$$a(p_h, \varphi_i) = \sum_l a(\varphi_l, \varphi_i) p_l.$$

From the definition of the basis functions φ_l , $a(\varphi_l, \varphi_i)$ equals zero unless \mathbf{x}_l and \mathbf{x}_i are the vertices of the same triangle. Thus the restriction of $a(p_h, \varphi_i)$ to each triangle $K \in K_h$ (cf. Fig. 2) has the form

$$a(p_h, \varphi_i)|_K = |K| \sum_{l=i,j,k} \nabla \varphi_l \cdot \nabla \varphi_i p_l,$$

which is exactly the right-hand side of (3.6) since $\varphi_l = \lambda_l$ on K . □

It follows from Lemma 6.1 that method (6.1) can be written: Find $p_h \in V_h$ such that

$$a(p_h, v) = (f, \hat{v}) \quad \forall v \in V_h. \tag{6.3}$$

Therefore, the sole difference between the standard finite element method (2.4) and the CVFE method (6.1) lies in the right-hand sides of these two equations.

Theorem 6.2. *Let K_h be a shape-regular triangulation of Ω , and let p and p_h be the respective solution of (2.3) and (6.3). Then*

$$|p - p_h|_{H^1(\Omega)} \leq Ch \|f\|_{L^2(\Omega)}. \tag{6.4}$$

Proof. Subtracting equation (6.3) from equation (2.4) gives

$$a(p_h^s - p_h, v) = (f, v - \widehat{v}) \quad \forall v \in V_h. \tag{6.5}$$

By the definition of \widehat{v} , we see that

$$(f, v - \widehat{v}) = \sum_{V_i} \int_{V_i} f(v - v_i) \, d\mathbf{x} = \sum_{V_i} \sum_{K \cap V_i \neq \emptyset, K \in K_h} \int_K f(v - v_i) \, d\mathbf{x}.$$

Consequently, since v is linear on each $K \in K_h$,

$$(f, v - \widehat{v}) \leq Ch \|f\|_{L^2(\Omega)} |v|_{H^1(\Omega)}.$$

Now, taking $v = p_h^s - p_h$ in (6.5) yields

$$|p_h^s - p_h|_{H^1(\Omega)} \leq Ch \|f\|_{L^2(\Omega)},$$

which, together with (2.5), implies inequality (6.4). □

7. Numerical Experiments. In this section we report a couple of examples for the CVFE methods. In the first example we check their accuracy, and in the second one they are applied to a two-phase flow problem in a porous medium. For more numerical experiments on the CVFE, please refer to [30, 31].

Table 1. Numerical results for p and \mathbf{u} .

$1/h$	$\ p - p_h\ _{L^2(\Omega)}$	rate	$\ \mathbf{u} - \mathbf{u}_h\ _{L^2(\Omega)}$	rate
2	0.18584850	-	1.2560773	-
4	5.8970002E-02	1.6561	0.68846096	0.8675
8	1.5744807E-02	1.9051	0.35305205	0.9635
16	4.0029721E-03	1.9757	0.17767979	0.9906
32	1.0049860E-03	1.9939	8.8985854E-02	0.9976
64	2.5151431E-04	1.9985	4.4511228E-02	0.9994

Example 1. Let $\Omega = (0, 1) \times (0, 1)$ be the unit square, \mathbf{a} be the identity tensor, and

$$f(\mathbf{x}) = 2\pi^2 \cos(\pi x_1) \cos(\pi x_2).$$

To be more general, the boundary conditions also include a Neumann portion:

$$\begin{aligned} \nabla p \cdot \boldsymbol{\nu} &= 0, & x_1 = 0 \text{ and } x_1 = 1, & \quad x_2 \in (0, 1), \\ p &= \cos(\pi x_1), & x_1 \in (0, 1), & \quad x_2 = 0, \\ p &= -\cos(\pi x_1), & x_1 \in (0, 1), & \quad x_2 = 1. \end{aligned}$$

Then the exact solution to (2.1) with these boundary conditions is

$$p = \cos(\pi x_1) \cos(\pi x_2).$$

Numerical errors and the corresponding convergence rates for p and its gradient $\mathbf{u} = \nabla p$ in the $L^2(\Omega)$ -norm are given in Table 1. From these computational results, we see that the convergence rates for p and \mathbf{u} are asymptotically of order $\mathcal{O}(h^2)$ and $\mathcal{O}(h)$, respectively, which is consistent with our theory established in the previous section.

Example 2. We now apply the CVFE to two-phase flow in a porous medium. The model presented is a general multi-dimensional model.

For the flow of two incompressible, immiscible fluids in a porous medium $\Omega \subset \mathbb{R}^d$ ($d \leq 3$), the mass balance equation for each of the fluid phases is [4, 13, 36]

$$\phi \frac{\partial(\rho_\alpha s_\alpha)}{\partial t} + \nabla \cdot (\rho_\alpha \mathbf{u}_\alpha) = \rho_\alpha q_\alpha, \quad \alpha = w, o, \tag{7.1}$$

where $\alpha = w$ denotes the wetting phase (e.g., water), $\alpha = o$ indicates the nonwetting phase (e.g., oil), ϕ is the porosity of the medium, and ρ_α , s_α , \mathbf{u}_α , and q_α are, respectively, the density, saturation, volumetric velocity, and external volumetric flow rate of the α -phase. The volumetric velocity \mathbf{u}_α is given by Darcy’s law

$$\mathbf{u}_\alpha = -\frac{\kappa \kappa_{r\alpha}}{\mu_\alpha} \nabla(p_\alpha - \rho_\alpha g Z), \quad \alpha = w, o, \tag{7.2}$$

where κ is the absolute permeability of the porous medium, p_α , μ_α , and $\kappa_{r\alpha}$ are the pressure, viscosity, and relative permeability of the α -phase, respectively, g denotes the gravitational constant, Z is the depth, and the x_3 -coordinate is in the vertical downward direction. In addition to (7.1) and (7.2), the customary property for the saturations is

$$s_w + s_o = 1, \tag{7.3}$$

and the two phase pressures are related by the capillary pressure function

$$p_c(\mathbf{x}, s_w) = p_o - p_w. \tag{7.4}$$

Finally, we define q_α in (7.1) by

$$q_\alpha = \sum_l q_\alpha^{(l)} \delta(\mathbf{x} - \mathbf{x}^{(l)}), \quad \alpha = w, o,$$

where $q_\alpha^{(l)}$ indicates the volume of the fluid produced or injected per unit time at the l th well, $\mathbf{x}^{(l)}$, for phase α and δ is the Dirac delta function. Following [37], $q_\alpha^{(l)}$ can be defined by

$$q_\alpha^{(l)} = \frac{2\pi \kappa \kappa_{r\alpha} \Delta L^{(l)}}{\mu_\alpha \ln(r_e^{(l)}/r_c^{(l)})} \left(p^{(l)} - p_\alpha - \rho_\alpha g (Z^{(l)} - Z) \right), \tag{7.5}$$

where $\Delta L^{(l)}$ is the length of the l th well, $p^{(l)}$ is the flowing bottom hole pressure at the (datum level) depth $Z^{(l)}$, $r_e^{(l)}$ is the equivalent radius, and $r_c^{(l)}$ is the radius of the l th well.

In this paper equations (7.1)–(7.5) are solved in an improved IMPES (implicit pressure-explicit saturation) manner. To separate the pressure and saturation equations, we introduce the phase mobility functions

$$\lambda_\alpha(\mathbf{x}, s_\alpha) = \kappa_{r\alpha}(\mathbf{x}, s_\alpha)/\mu_\alpha, \quad \alpha = w, o,$$

and the total mobility

$$\lambda(\mathbf{x}, s) = \lambda_w + \lambda_o,$$

where $s = s_w = 1 - s_o$. The fractional flow functions are defined by

$$f_\alpha(\mathbf{x}, s) = \lambda_\alpha/\lambda, \quad \alpha = w, o.$$

Following [3, 7], we define the global pressure as

$$p = p_o - \int^s (f_w \frac{\partial p_c}{\partial s})(\mathbf{x}, \xi) d\xi. \tag{7.6}$$

Finally, we define the total velocity

$$\mathbf{u} = \mathbf{u}_w + \mathbf{u}_o. \quad (7.7)$$

Now, under the assumption that the fluids are incompressible we apply (7.3) and (7.7) to (7.1) to see that

$$\nabla \cdot \mathbf{u} = q(p, s) \equiv q_w + q_o, \quad (7.8)$$

and (7.4), (7.6), and (7.7) to (7.2) to obtain

$$\mathbf{u} = -\kappa(\lambda(s)\nabla p + \gamma_1(s)), \quad (7.9)$$

where

$$\gamma_1 = -\lambda_w \nabla_{\mathbf{x}} p_c + \lambda \int^s \nabla_{\mathbf{x}} (f_w \frac{\partial p_c}{\partial s})(\mathbf{x}, \xi) d\xi - (\lambda_w \rho_w + \lambda_o \rho_o) g \nabla Z.$$

Similarly, apply (7.4), (7.6), (7.9), and the constant densities to (7.1) and (7.2) with $\alpha = w$ to obtain

$$\phi \frac{\partial s}{\partial t} + \nabla \cdot \left\{ \kappa f_w(s) \lambda_o(s) \left(\frac{\partial p_c}{\partial s} \nabla s + \gamma_2(s) \right) + f_w(s) \mathbf{u} \right\} = q_w(p, s), \quad (7.10)$$

where

$$\gamma_2 = \nabla_{\mathbf{x}} p_c - (\rho_o - \rho_w) g \nabla Z.$$

In (7.8) and (7.10), the well terms are now defined in terms of the global pressure p and saturation s :

$$q_{\alpha}^{(l)}(p, s) = \frac{2\pi\kappa\kappa_r\alpha\Delta L^{(l)}}{\mu_{\alpha} \ln(r_e^{(l)}/r_c^{(l)})} \left(p^{(l)} - p - \gamma_{\alpha} - \rho_{\alpha} g (Z^{(l)} - Z) \right), \quad (7.11)$$

where

$$\gamma_o = \int^s (f_w \frac{\partial p_c}{\partial s})(\mathbf{x}, \xi) d\xi, \quad \gamma_w = \int^s (f_w \frac{\partial p_c}{\partial s})(\mathbf{x}, \xi) d\xi - p_c.$$

The pressure equation is given by (7.8) and (7.9), while the saturation equation is described by (7.10). They determine the main unknowns p , \mathbf{u} , and s . The model is completed by specifying boundary and initial conditions. In this paper we consider no-flow boundary conditions

$$\begin{aligned} \mathbf{u} \cdot \boldsymbol{\nu} &= 0, & \mathbf{x} &\in \Gamma, \\ \left\{ \kappa f_w(s) \lambda_o(s) \left(\frac{\partial p_c}{\partial s} \nabla s + \gamma_2(s) \right) + f_w(s) \mathbf{u} \right\} \cdot \boldsymbol{\nu} &= 0, & \mathbf{x} &\in \Gamma. \end{aligned} \quad (7.12)$$

The initial condition is given by

$$s(\mathbf{x}, 0) = s_0(\mathbf{x}), \quad \mathbf{x} \in \Omega. \quad (7.13)$$

The differential system has a clear structure; the pressure equation is elliptic for p and the saturation equation is parabolic for s . The parabolic equation is degenerate in the sense that the capillary diffusion coefficient $\kappa f_w \lambda_o \partial p_c / \partial s$ can be zero. These two equations are nonlinear. The mathematical properties of this system such as existence, uniqueness, regularity, and asymptotic behavior of solutions have been studied in [9, 10].

The global pressure p in (7.6) is used. The use of this variable reduces the coupling between pressure and saturation equations [11]. It is also convenient in the treatment of wells, as in (7.11). Also, in the case where f_w and p_c depend only on s , it follows from (7.4) and (7.6) that

$$\lambda \nabla p = \lambda_w \nabla p_w + \lambda_o \nabla p_o.$$

This implies that the global pressure is the pressure that would produce the flow of a fluid (with mobility λ) equal to the sum of the flows of fluids w and o .

It follows from (7.8) and (7.9) that

$$-\nabla \cdot [\kappa(\lambda(s)\nabla p + \gamma_1(s))] = q(p, s).$$

This pressure equation is solved implicitly:

$$-\nabla \cdot [\kappa^n(\lambda(s^n)\nabla p^n + \gamma_1(s^n))] = q(p^n, s^n), \tag{7.14}$$

where p^n represents the value of p at time level t^n . On each control volume V_i , we have

$$-\int_{\partial V_i} \kappa^n(\lambda(s^n)\nabla p^n + \gamma_1(s^n)) \cdot \nu \, d\ell = \int_{V_i} q(p^n, s^n) \, d\mathbf{x}, \tag{7.15}$$

to which the CVFE applies.

The saturation equation (7.10) is solved explicitly in time:

$$\phi \frac{s^{n+1} - s^n}{\Delta t^{n+1}} + \nabla \cdot \{ \kappa^n f_w(s^n) \lambda_o(s^n) (\frac{\partial p_c^n}{\partial s} \nabla s^n + \gamma_2(s^n)) + f_w(s^n) \mathbf{u}^n \} = q_w(p^n, s^n),$$

where Δt^{n+1} is the time step at level t^{n+1} and

$$\mathbf{u}^n = -\kappa^n(\lambda(s^n)\nabla p^n + \gamma_1(s^n)).$$

Again, as in (7.15) we see that, on each V_i ,

$$\int_{V_i} \phi \frac{s^{n+1} - s^n}{\Delta t^{n+1}} \, d\mathbf{x} + \int_{\partial V_i} \{ \kappa^n f_w(s^n) \lambda_o(s^n) (\frac{\partial p_c^n}{\partial s} \nabla s^n + \gamma_2(s^n)) + f_w(s^n) \mathbf{u}^n \} \cdot \nu \, d\ell = \int_{V_i} q_w(p^n, s^n) \, d\mathbf{x}. \tag{7.16}$$

An improved IMPES procedure [12] is used to solve (7.15) and (7.16). This procedure utilizes an adaptive control strategy on the choice of the time step for the saturation and takes a much larger time step for the pressure than for the saturation. Through a stability analysis and a comparison with a simultaneous solution procedure, we have shown that this improved procedure is effective and efficient for the numerical simulation of two-phase flow and it is capable of solving two-phase coning problems [12].

Table 2. Relative permeability data.

s	κ_{rw}	κ_{ro}
0.22	0	1
0.3	0.07	0.4
0.4	0.15	0.125
0.5	0.24	0.0649
0.6	0.33	0.0048
0.8	0.65	0
0.9	0.83	0
1	1	0

This numerical example is chosen to check the applicability of the CVFE to two-phase (water and oil) flow in a porous medium. The absolute permeability κ is 100 md, the porosity is $\phi = 0.2$, and the medium dimensions are $1,050 \times 866 \times 100 \text{ ft}^3$ (the flow is two-dimensional; i.e., it is uniform in the x_3 -direction and the gravity is ignored). There are five wells: a water injection located at the center (525.00 ft, 433.00 ft) and four production wells located at (75.00 ft, 779.42 ft),

(975.00 ft, 779.42 ft), (75.00 ft, 86.60 ft), and (975.00 ft, 86.60 ft). The bottom hole pressures at injection and production wells are 3,700 psi and 3,500 psi, and the water and oil viscosities are 0.4 cp and 6.0 cp, respectively. The relative permeability data are given in Table 2 and the capillary pressure is zero. The initial condition is $s_0 = 0.2$. The harmonic average is used for the absolute permeability κ , while the flux-based upstream weighting scheme is used for the phase and total mobilities, λ_α and λ , $\alpha = w, o$.

The grid size is chosen to be 50 ft between the centers of adjacent control volumes, and the choice of time steps (in terms of a few days) is given as in [12]. We use a saturation profile to check the grid orientation effect, which is shown in Fig. 6 at 217 days. From this figure, we see that the water front is a circle. This implies that water spreads in the same speed in all directions, and thus the CVFE does not have an orientation effect.

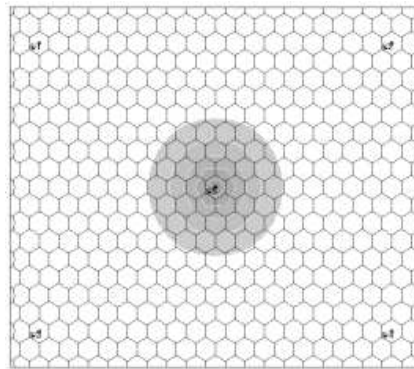


Fig. 6: The saturation at 217 days by the CVFE.

8. Concluding Remarks. We have systematically studied the CVFE methods for numerical solutions of second-order partial differential equations. Their relationships to the finite difference and standard finite element methods are discussed. Through their relationship to the finite differences, the upstream weighted CVFE methods and the conditions on positive flux linkages are considered, and through their relationship to the standard finite elements, error estimates for the CVFE methods are obtained. These estimates are comparable to those for the standard finite element methods. Numerical experiments performed support the mathematical theory derived in this paper. A two-phase flow application shows that the CVFE methods are useful in reducing grid orientation effects.

Acknowledgements. The author would like to thank Professor Guanren Huan and Dr. Baoyan Li for providing some of the numerical experiments in this paper.

REFERENCES

- [1] I. Aavatsmark, E. Reiso, and R. Teigland, *Control-volume discretization method for quadrilateral grids with faults and local refinements*, *Computational Geosciences*, **5** (2001), 1–23.
- [2] R. A. Adams, “Sobolev Spaces,” Academic Press, Inc., New York, 1975.
- [3] S. N. Antontsev, *On the solvability of boundary value problems for degenerate two-phase porous flow equations*, *Dinamika Splošnoi Sredy Vyp.*, **10** (1972), 28–53, in Russian.
- [4] K. Aziz and A. Settari, “Petroleum Reservoir Simulation,” Applied Science, Publishers Ltd, London, 1979.

- [5] R. E. Bank and D. J. Rose, *Some error estimates for the box method*, SIAM J. Numer. Anal., **24** (1987), 777–787.
- [6] Z. Cai, J. Mandel, and S. McCormick, *The finite volume element method for diffusion equations on general triangulations*, SIAM J Numer Anal., **28** (1991), 392–403.
- [7] G. Chavent and J. Jaffré, *Mathematical Models and Finite Elements for Reservoir Simulation*, North-Holland, Amsterdam, 1978.
- [8] Z. Chen, *Analysis of mixed methods using conforming and nonconforming finite element methods*, RAIRO Model. Math. Anal. Numer., **27** (1993), 9–34.
- [9] Z. Chen, *Degenerate two-phase incompressible flow I: Existence, uniqueness and regularity of a weak solution*, Journal of Differential Equations, **171** (2001), 203–232.
- [10] Z. Chen, *Degenerate two-phase incompressible flow II: Regularity, stability and stabilization*, Journal of Differential Equations, **186** (2002), 345–376.
- [11] Z. Chen and R. E. Ewing, *Comparison of various formulations of three-phase flow in porous media*, J. Comp. Physics, **132** (1997), 362–373.
- [12] Z. Chen, G. Huan, and B. Li, *An improved IMPES method for two-phase flow in porous media*, Transport in Porous Media, **54** (2004), 361–376.
- [13] Z. Chen, G. Huan, and Y. Ma, “Computational Methods for Multiphase Flows in Porous Media,” in the Computational Science and Engineering Series, Vol. 2, SIAM, Philadelphia, PA, 2006.
- [14] Z. Chen and J. Li, *A new stabilized finite volume method for the stationary Stokes equations*, submitted for publication.
- [15] Z. Chen, R. Li, and A. Zhou, *A note on the optimal L^2 -estimate of finite volume element method*, Adv. Comput. Math., **16** (2002), 291–303.
- [16] S. H. Chou and D. Y. Kwak, *Analysis and convergence of a MAC scheme for the generalized Stokes problem*, Numer. Meth. Partial Diff. Equ., **13** (1997), 147–162.
- [17] S. H. Chou and D. Y. Kwak, *A covolume method based on rotated bilinears for the generalized Stokes problem*, SIAM J. Numer. Anal., **35** (1998), 494–507.
- [18] S. H. Chou and Q. Li, *Error estimates in L^2 , H^1 and L^∞ in control volume methods for elliptic and parabolic problems: a unified approach*, Math Comp., **69** (2000), 103–120.
- [19] S.-H. Chou and P. S. Vassilevski, *A general mixed covolume framework for constructing conservative schemes for elliptic problems*, Math. Comp., **68** (1999), 991–1011.
- [20] P. G. Ciarlet, “The Finite Element Method for Elliptic Problems,” North-Holland, Amsterdam, 1978.
- [21] E. F. D’Azevedo and R. B. Simpson, *On optimal interpolation triangle incidences*, SIAM J. Sci. Stat. Comput., **10** (1989), 1063–1075.
- [22] R. E. Ewing (ed.), “The Mathematics of Reservoir Simulation,” SIAM, Philadelphia, 1983.
- [23] R. E. Ewing, T. Lin, and Y. Lin, *On the accuracy of the finite volume element method based on piecewise linear polynomials*, SIAM J. Numer. Anal., **39** (2002), 1865–1888.
- [24] P. A. Forsyth, *A control volume finite element approach to NAPL groundwater contamination*, SIAM J. Sci. Stat. Comput., **12** (1991), 1029–1057.
- [25] L. S. Fung, A. D. Hiebert, and L. Nghiem, “Reservoir Simulation with a Control Volume Finite Element Method,” SPE 21224, the 11th SPE Symp. Reser. Simul., Anaheim, 1991.
- [26] B. Heinrich, “Finite Difference Methods on Irregular Networks,” Birkhauser, Basel, Boston, Stuttgart, 1987.
- [27] B. Joe, *Delaunay triangular meshes in convex polygons*, SIAM J. Sci. Stat. Comput., **7** (1986), 514–539.
- [28] R. D. Lazarov, I. D. Mishev, and P. S. Vassilevski, *Finite volume methods for convection-diffusion problems*, SIAM J. Numer. Anal., **33** (1996), 31–55.
- [29] P. A. Lemonnier, *Improvement of reservoir simulation by a triangular discontinuous finite element method*, SPE paper 8249 presented at the 1979 Annual Fall Technical Conference and Exhibition of SPE of AIME, Las Vegas, Sept. 23–26.
- [30] B. Li, Z. Chen, and G. Huan, *Control volume function approximation methods and their applications to modeling porous media flow I: The two-phase flow*, Advances in Water Resources, **26** (2003), 435–444.
- [31] B. Li, Z. Chen, and G. Huan, *Control volume function approximation methods and their applications to modeling porous media flow II: The black oil model*, Advances in Water Resources, **27** (2004), 99–120.
- [32] R. Li, *Generalized difference methods for a nonlinear Dirichlet problem*, SIAM J Numer Anal., **24** (1987), 77–88.

- [33] R. Li, Z. Chen, and W. Wu, "The Generalized Difference Method for Differential Equations-Numerical Analysis of Finite Volume Methods," Marcel Dekker, New York, 2000.
- [34] R. Li and P. Zhu, *Generalized difference methods for second order elliptic partial differential equations (I) (in Chinese)*, Numer. Math., **4** (1982), 140–152.
- [35] C. Liu and S. McCormick, *The finite volume element method (FVE) for planar cavity flow*, Proc. 11th Internat. Conf. on CFD, Williamsburg, VA, June 28–July 2, 1988, 365–387.
- [36] D. W. Peaceman, "Fundamentals of Numerical Reservoir Simulation," Elsevier, New York, 1977.
- [37] D. W. Peaceman, "Interpretation of Well-block Pressures in Numerical Reservoir Simulation," SPE 6893, 52nd Annual Fall Technical Conference and Exhibition, Denver, 1977.
- [38] H. Rui, *Analysis on a finite volume element method for the Stokes problems*, Acta Mathematicae Applicatae Sinica, English Series, **3** (2005), 359–372.
- [39] R. S. Varga, "Matrix Iterative Analysis," Prentice-Hall, Englewood Cliffs, NJ, 1962.
- [40] S. Verma and K. A. Aziz, *Control volume scheme for flexible grids in reservoir simulation*, Paper SPE37999, the 1997 SPE Symposium on Reservoir Simulation, Dallas, June 8-11, 1997.
- [41] X. Ye, *On the relationship between finite volume and finite element methods applied to the Stokes equations*, Numer. Methods Partial Diff. Equ., **5** (2001), 440–453.

Received for publication September 2006.

E-mail address: `zchen@mail.smu.edu`